sciendo

PRODUCTION ENGINEERING ARCHIVES 2023, 29(2), 201-215

PRODUCTION ENGINEERING ARCHIVES

ISSN 2353-5156 (print)
ISSN 2353-7779 (online)

Exist since 4th quarter 2013
Available online at https://pea-journal.eu

Design and optimization of the construction of a mobile disinfection chamber for small communication devices and small objects

Ján Galík[1*], Daniel Varecha[1], Mário Drbúl[2], Rudolf Madaj[3], Viera Konstantová[3]

[1] Research and service center, Faculty of Mechanical engineering, University of Žilina, Univerzitná 8215/1, 010 26 Žilina, Slovak republic; jan.galik@fstroj.uniza.sk (JG) daniel.varecha@ fstroj.uniza.sk (DV)
[2] Department of Machining and Production Technologies, Faculty of Mechanical engineering, University of Žilina, Univerzitná 8215/1, 010 26 Žilina, Slovak republic; mario.drbul@ fstroj.uniza.sk
[3] Department of Design and Machine Elements, Faculty of Mechanical engineering, University of Žilina, Univerzitná 8215/1, 010 26 Žilina, Slovak republic; rudolf.madaj@ fstroj.uniza.sk (RD), viera.konstantova@ fstroj.uniza.sk (VK)
*Correspondence: jan.galik@fstroj.uniza.sk, Tel.: + 421 910 746 751, +421 41 513 2931

Article history
Received 25.08.2022
Accepted 28.11.2022
Available online 08.05.2023

Keywords
Pathogens
UV-C radiation
Disinfection
Additive manufacturing
Rapid prototyping

Abstract
This manuscript aims to familiarise readers with the development of a device for the construction of a mobile disinfection chamber for small communication devices and small objects. The conceptual design and the material of the new device play essential roles in the design process of a new device. The manuscript presents concepts based primarily on previous experience and different perspectives. The concept design is created in the 3D modelling program CREO Parametric 8.0. A multi-criteria team evaluation determined the most suitable version of the idea. For dimensioning and shape adaptation of the device was used EinScan SP device (3D scanning method). The article's aim was also to establish a suitable way of producing a prototype using tribological research in available production methods and materials within rapid prototyping. Using the ALICONA Infinite Focus G5 device, experimentally investigated the parameters characterising the surface of the parts. The end of the manuscript focused on the mechanical structure and subjecting them to FEM analysis in the program ANSYS Workbench. The design of the concept disinfection device was also for extreme cases of use. Within this issue was optimising shapes, wall thicknesses, reinforcement design and other necessary modifications using the FEM analysis. From the results, the most suitable material to produce a more significant number of parts may not be the most suitable material to create prototype devices. Tools such as 3D scanning, rapid prototyping, and FEM analysis can "significantly" help reduce mistakes before testing the device.

DOI: 10.30657/pea.2023.29.24

1. Introduction

Modern technologies such as 3D printing and 3D scanning of objects bring a new perspective to the production sphere. These tools significantly speed up the prototyping process. At the same time, new knowledge in the given industries makes it possible to simplify the prototyping process even more. The last two years have shown the fragility of people's health. Achieving health protection is possible in different ways. One of the most effective methods is to keep the environment around us free of harmful germs, clean drinking water, and disinfect surfaces (National Environment Agency, 2021). These factors can fundamentally impact a person's health and mental and physical well-being. (Ooster-hoff and Palmet, 2020) Various bacteria, viruses or fungi pose a threat to each of us. We often encounter such micro-organisms in everyday life when we meet several people, for example, at work, restaurants, shops, schools, museums, public transport, bars, etc. Recent years (especially from 2020) have shown that humans are vulnerable to new pathogens. (Chen et al., 2020; Baloch et al., 2020; Wu et al., 2020) One of the diseases that significantly affected our lives was the infectious SARS-CoV-2 virus (COVID-19), the spread of which the entire world opposed. (European Council, 2022) According to Morawska and

Cao (2020) and Lewis (2020), the infection can be e. g. like, COVID-19, even by individuals without symptoms.

The main recommendations for preventing infection are frequent ventilation, air disinfection, and minimization of contact. (Morawska and Cao, 2020) According to the Centres for Disease Control and Prevention (CDC), it is possible to use the so-called pyramid of hierarchy, where among the most effective ways to protect a person is to eliminate the danger of infection and the spread of pathogens. (CDC, 2015), Of course, the human ability to resist pathogens cannot be forgotten. The defence of the body can be supported by a sufficient level of vitamin D (Nourazzaran et al., 2022; Groth, 2020), a healthy diet (FAO et al., 2020), and sufficient sleep and rest (Luyster et al., 2012).

One of the most effective ways to protect people against pathogens is the disinfection of surfaces, air, hands, parts of objects, and the environment. Disinfection can occur in various ways. (CDC, 2021; Bukłaha et al., 2022) Disinfection using ultraviolet (UV) radiation is coming to the fore, specifically UV-C. Philips (2022) company has been developing this technology and its application to various devices that facilitate daily life for a long time. UV-C alone can disinfect surfaces by up to 99,9% in the case of COVID-19, with a short exposure time. (Ma et al., 2021; Kitagawa et al., 2021) Different sources of UV-C radiation (Light-emitting diode- LED, excimer lamps, tubes...) at different wavelengths (200-280nm) are used for the disinfection process. (Ruschel et al., 2020) (Sharma et al., 2021) According to Bergman (2021), Krypton chloride gas (KrCl*) discharge lamps are one of the most appropriate sources of UV-C because they emit a wavelength (222 nm) that does not harm human cells, the so-called "UV-C light lamp". LEDs that emit light ranging from 254 to 280 nm are promising for measuring dimensions and weight. Diodes are not very efficient (4-5%) and are still being developed. (Hsu et al., 2021) When creating and designing concepts for new devices, it is essential to identify the needs and the way electro-optical, mechanical, and thermal components work together (Sharma et al., 2021; JAG, 2020).

The main of this article theme is the design a device that, with its mobility and functionality, would help mitigate the effects of the spread of various types of pathogens in the human population. By using this device, pathogens would be destroyed in the buds on small objects of daily use. Items include small communication devices (mobile phones), wallets, keys, remote controls, watches, and others. The device's compactness should be combined with a simple and intuitive disassembly. Low weight is essential for the device's mobility and directly impacts the user and his decision to take such a device with him for everyday use. Combining these features makes it possible to create a concept that can be successful. There is a fast way to move from the idea to an actual mechanical prototype. Components (proto-types) can be produced using conventional (CNC milling, turning, casting, injection, etc.) and unconventional methods (rapid prototyping, laser machining, water jet machining, electro-erosive machining, and many other ways). (StudentLesson, 2022) It largely depends on the material required from which the prototype will be made. This idea was based on the production and economic complexity of the new prototype (Gibson et al., 2014).

The concept of the device should be as compact as possible with low weight. The additive manufacturing method is ideal for producing a prototype and verifying the functionality of a printed-out component. The product made using this method is a preliminary mechanical version. It is necessary to emphasize the essential characteristics of these products. (Wiberg et al., 2021; Obi et al., 2022) Concept designers can verify the design's suitability and the operation principle and provide the resulting product specifications. (engineeringproductdesign, 2022)

The variety of manufacturing methods using additive 3D printing is incredible and opens many opportunities for its use. The history of this production method dates to the 80s and 90s. The most significant expansion occurred at the turn of the millennium, especially in the USA. (Ouajjani, 2018) The efforts of the European Space Agency (ESA) in the project Additive Manufacturing Aiming Towards Zero Waste & Efficient Production of High-Tech Metal Products (AMAZE) come to people's attention. (ESA, 2013) Precisely because of the efficiency and printing of shapes that are often difficult to produce, producing parts using additive technology is the ideal way of making prototype parts. (Khorasani et al., 2022)

The proposed device should be used to disinfect small items for daily use. For the size optimization of the device, the 3D scanning method was used in other parts of the article. Specifically, it involves the use of the multifunctional scanner EINSCAN SP. (SHINING 3D, 2022) By comparing, scanning, and inserting objects into the device, new suggestions for shaping can be made (see Chapter 3.1). Using a 3D scan can change the device and optimize it to the required shape – size. Using the Final element method (FEM), it is possible to perform arrival analyses at critical points to preserve the device's functionality (see Chapter 4).

Additive manufacturing can use different methods and innovative, light, and intelligent materials (4D printing). (Gibson et al., 2014; Mohol and Sharma, 2021; Furka et al., 2021) A suitable method of making the prototype was selected by comparing three prints from different printers. The printers reached in Section 3.2 are Sinterit LISA (Sinterit, 2022), EOS FORMIGA P100 (EOS, 2007), and HP JET Fusion 4200 (HP, 2022). Subsequently, the samples were subjected to optical micro coordinate measurement and measurement of surface properties using the ALICONA Infinite-Focus G5 device. (ALICONA, 2022) The evaluation of the samples considers the surface in terms of functionality, execution, and roughness. The results of this research should provide a conceptual design with an actual model prototype of a mobile device for disinfecting small objects.

2. Proposal of solution Variants

In the introduction, several features which should characterize the concept of the newly designed device were described. Similar devices based on a similar principle of UV-C radiation (Philips UV-C, 2022) are, e. g. from the Philips company with a volume of 10 litres (288.2 mm x 288.2 mm x 285.1 mm)

(Philips Box, 2022) and a Mini box of compact dimensions (234mm x 150mm x 127mm). (Philips Mini box, 2022) These devices are of a high level of processing. It is necessary to orient the new device concept towards simple collapsibility and intuitive assembly to increase mobility. These properties must be combined with low weight. The ratio of the economic complexity of the structure linked to the body of the device cannot be neglected. The intuitiveness of the use and control of the device should be high. UV-C radiation from the device must not be in direct contact with the skin (completely covered). The main requirements of the construction are summarized in Table 1.

Table 1. Requirements for a new facility concept

New device characteristics	
a) Disinfection with UV-C radiation	Must be
b) Biocompatibility	Must be
c) High degree of mobility	Wish
d) High security	Must be
e) Intuitive control	Must be
f) The most diminutive dimensions	Wish
g) Price Availability	Wish
h) Low operating costs	Must be
i) A small number of components	Wish
j) Resistance to external influences	Wish

The following Section describes the design solutions for a given problem. Each of the presented concepts is an approximate design solution. The visualization of the variants has been created in the software CREO 8.0.

2.1. "Pull-out box" concept

Concept number 1 is based on the principle of inserting one part into another, creating a telescopic extension mechanism. In Figure 1, it is possible to see the concept in an exploded state.

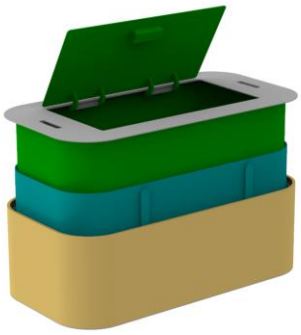

Fig. 1. The concept of "Pull-out box" in the open state

Within the framework of the presented structure, it is possible to increase the device's disinfection space by two to three times compared with the original state. In this construction is a problem with locking mechanisms. The upward extension is opposed by the force of gravity, which pulls all telescopic links of the device downwards. The widget needs the guidance of individual cells in an up-down direction. With this variant, there is a problem with the solution of illuminating objects using UV-C radiation owing to the layout and extension mechanism. According to this concept, UV-C light sources can only be placed in the lower part of the device. Radiation only in the lower part can negatively affect the rate of disinfection of objects placed in the device and the length of stay.

2.2. "Matchbox" concept

The "matchbox" concept is a possible way to approach the request for a new device concept (see Figure 2). One of the most significant advantages is the ease of use. After the central part is extended and the device is opened, objects can be inserted. This concept can only be used in an unfolded state compared to the previous variant. The solution of the opening mechanism and hinges allows the device to be opened on a larger scale, directly impacting the insertion and removal of the device. Securing the opening mechanism can be e. g. using mechanics (locking pin) or a glued magnet. The placement of UV-C radiation sources was only possible in the central region (blue part). Therefore, the length of exposure of specific objects to radiation must be considered based on the dimensions and placement of a device.

Fig. 2. The concept of "Matchbox" in the open state

2.3. "Folding box" concept

The third concept is based primarily on the idea of the collapsibility and assembly of the device. Reducing the device to the smallest possible size brings a great benefit. By increasing compliance and reducing weight, increased device portability and mobility can be achieved. By using folding sides on the sides and one folding side on both fronts of the device, the necessary assembly and intuitive use of the device can be achieved (see Figure 3).

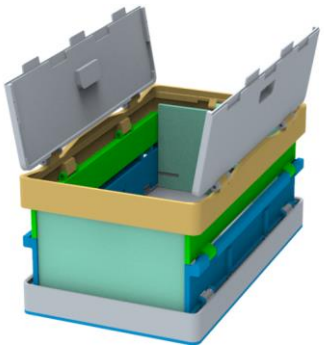

Fig. 3. The concept of "Folding box" in the open state

The opening uses an upper pair of doors through which the user enters the internal storage space. Locking in folded and unfolded positions can be done using magnets. As described in the introduction, an advantage of this concept is its compactness combined with its low weight and mobility. The disadvantage of this concept is the inability to use the device in a folded state. The space in the lower part of the device is for the power supply.

2.4. Evaluation of concepts

For a relatively impartial evaluation and selection of the best variant to produce the prototype within the college of researchers, concepts were presented, and the evaluation participants performed the so-called multi criteria evaluation. The participants (authors) assigned values from 1 to 5 for each variant. The highest values indicated the best assessment for the criterion's weight and for assessing a specific variant's abilities. The individual requirements were averaged using the criteria weight (from 1 to 10) in the given assessment. The results are summarized in Table 2.

Table 2. Evaluation of variants

Comparison of variants				
Characteristics	Weight	VAR 1	VAR 2	VAR 3
Consistency	8	3	3	5
UV-C effect	7	2	3	3
Usability	6	3	3	4
Weight	8	2	3	4
Constr. complexity	7	4	3	3
Economic difficulty	6	3	3	3
Biolog. interaction	5	3	3	3
Sum		19	21	**25**

It follows from the multi-criteria evaluation that the evaluation of variant 3 surpassed that of other variants and will be optimized for specific use in subsequent steps. The complexity of the construction can be understood as an effort to minimize the number of individual parts. The mentioned condition can only be fulfilled to a certain "reasonable" extent owing to the collapsibility of the device.

Another essential component is the solution for the power supply, control, and distribution of the electrical module, which should closely cooperate with the structural part. (Tropp et al., 2017) The resulting device prototype may not meet all relevant requirements if this element is not well combined. As part of the creation of the prototype, it is necessary to apply comments from electricians and prepare the structure for the given requirements. For the initial prototype and testing of the device, LEDs powered by a simple source are considered. A more complex device design (different functions of the control module, various supply voltages for the LEDs) will need to be combined with creating the printed circuit board (PCB).

3. Shape optimisation of the concept and production method

The first part of the optimization process involves measuring, scanning, and applying the scanned objects to a specific device model (Chapter 3.1). After 3D scanning and deter-mining the maximum dimensions of the disinfected objects and the box itself, it is necessary to define production technology. Chapter 3.2 deals with rapid prototyping. Based on an assessment of suitability for use, properties, and costs, a variant of the prototype production method was selected.

3.1. Scans of objects (3D scanning)

Scanning objects in space and their subsequent digitization provides designers with a powerful tool in the design process. Creating a digital form of a specific thing offers the possibility of digitizing things, such as daily needs. By digitizing objects, it is possible to obtain an idea of space requirements. These findings are essential for optimizing the shapes and dimensions of the prototype.

Object scanning was performed using the EinScan SP scanner. The device's performance was sufficient for scanning small objects (minimum object size 30 mm x 30 mm x 30 mm), with an accuracy of 0.05 mm. Scanning on the given device is possible with one click by placing the object to be scanned on a rotating stand, with a maximum stand load of 5kg (see Figure 4). (SHINING 3D, 2022)

Fig. 4. Scanner EinScan SP

Examples of 3D scans include a pen case with maximum dimensions of 130 mm x 50 mm x 20 mm. For the mobile phones, the full size was intended to be 150x76x15mm space. From this point of view, objective forms of objects are essential when optimizing and designing the device's interior for better imagination, visualization, and measurements. Scanning imperfections are caused by the reflection of surfaces from the beams of the scanner. Using the chalk spray eliminated a large part of the deficiencies. It can be seen in Figure 5 that the size of the chamber fit is adequate, with sufficient margins. The inner chamber of the device is formed with a 170 mm x 94 mm x 50 mm space. The outer part measure 190 mm x 110 mm x 86 mm when unfolded. The given dimensions include many different small objects. Daily use from keys, minor and medium-sized mobile phones, stationery, pen cases, wallets, and many others.

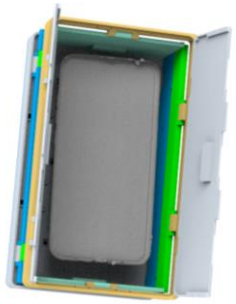

Fig. 5. Scanned mobile phone in UV-C disinfection box

3.2. Production methods of additive manufacturing

Current production technologies have shifted from conventional methods to modern and low-cost strategies. One of the most proclaimed methods that have come to the fore and have a primary position is the 3D printing of plastics, metals, carbon fibres, etc. Producing prototypes for the user is not complicated, and it is enough to have a 3D model. (Kohár et al., 2019) To create device prototypes, are available devices:

- Sinterit LISA
- EOS Formiga P100
- HP JET Fusion 4200

Two printers (LISA, EOS) are located within the University of Žilina, and one is in the friendly company of the University (HP). The first two printers operate using SLS (selective laser sintering) technology. The third printer (printing centre) works on the Multi-Jet Fusion (MJF) principle. By comparing these technologies precisely, the properties of the prints, selecting the type of technology and material that could be used was necessary. Printers use different types of plastics, such as PP, PA12, and PA11, or a combination of materials. (Mehrpouya et al., 2022) Before comparing printers, it is essential to note that each manufacturer provides its semi-finished powder for production. Therefore, devices that could give the prints similar characteristics were selected for comparison.

One of the first possible variants of the production of the prototype was using a SINTERIT LISA printer. This technology uses a laser as a heat source and selectively melts the powder on the individual layers. The laser focuses on the points in the given cross-sectional layer, as defined by the 3D model. The great advantage of this method is that the manufactured parts do not require supports that support protruding or isolated areas and layers. (Gibson et al., 2014; Gan et al., 2020) Due to its size (620 mm x 400 mm x 660 mm), compactness, and economic availability, the SINTERIT LISA device belongs to devices for small businesses. The maximum free volume for printing had dimensions of 110 mm x 160 mm x 130 mm. The full power of the laser used for the sintering was 5 W. The thickness of the printed layer is from 0.075-0.175 mm at a printing speed of 3mm/h (Sinterit, 2022).

Another available option for prototype printing is the EOS FORMIGA P100 printer, which uses the same method as the previous printer (SLS). Compared with the last printer, it is several times larger in size. The device is 1320 mm x 1067 mm x 2204 mm with an available print volume of 200 mm x250 mm x 330 mm. The laser power was more significant, up to 30 W. Depending on the material, the typical thickness of one layer is usually 0.1 mm. The size of the device and the print volume indicate the possibility of producing a small series of parts. Production is economically less demanding than in previous printers. The minimum thickness of the printed wall is 0,4 mm at a printing speed (depending on the material) of approximately 24 mm/h (EOS, 2007).

In 2016, came on the market technology from the HP company called MJF (Multi Jet Fusion). It stands out for its relative youth compared with competing and older technologies. Compared to these methods, a method of operation uses powder material in fusion with printing agents and heat applications. Initially, the space for applying the powder was heated evenly. After the powder was heated, it was selectively used. A detailed agent is used around the perimeter of the outer contours. As the lamps passed over the used powder, the sprayed material trapped the heat and distributed it evenly. The process of creating one layer of components occurred. (materialise, 2022) After the process is completed, the magazine is removed (the printing speed of the entire magazine is 10,5 hours) with the printed part/s and the remaining powder. Finally, the parts were brushed, and the remaining material was vacuumed into the hopper for further printing. (Sculpteo, 2021) The whole system provides high productivity. (HP, 2022) Based on the summary of the available printing methods, Table 3 was prepared. The table summarises all essential properties of the materials from which the prototype can be fabricated (in the hardened state).

Table 3. Comparison of properties of printed materials

Properties	Types of printers and materials					
Printer	Sinterit LISA		EOS FORMIGA P100		HP JET Fusion 4200	
Material	PA 12 Smooth		PA 2200		PA 12 (MJF)	
Characteristics	Norm	Value	Norm	Values	Norm	Value
Granule size		18-90 μm	ISO 13320-11	56 μm	ASTM D3418	60 μm
Density	EN ISO 845:2010	1g/cm^3	EOS method	0.93g/cm^3	ASTM D792	1.01g/cm^3
Tensile strength	EN ISO 37:2007	41MPa	EN ISO 527	48 MPa	ASTM D638	48 MPa
Elongation at break	ISO 37:2007	13%	EN ISO 527	24%	ASTM D638	X-20%; Y- 15%
Shore D – hardness	EN ISO 845:2010	74	ASTM D2240	75	ASTM D2240	80
Charpy – Impact strength	Internal proced.	15-20 kJ/m^2	EN ISO 179	32.8 kJ/m^2	EN ISO 179-1	35 kJ/m^2

As part of the investigation of printed parts, older prints from printers (SINTERIT, EOS, and HP) were subjected to surface analysis. The printed components were fabricated in the current printer settings. Samples of prints from these printers were subjected to microstructure observation under a microscope at 10x magnification using an Olympus SZX 16 Microscope. The macrostructures of the given surfaces were examined while observing the prints. Through sighting, it was found that the SINTERIT LISA printer provided a solid surface that was pleasant to touch. Surface structures were evident in the remaining two printers. The printer from the EOS used a white material in 3D printing, which was rougher with a visible structure even after sandblasting. When printed by the MJF method, the details of the surface structure were not visible, but the material was more integral from a macrostructural point of view than the product of the EOS printer.

The output from the Sinterit LISA printer is the material (Polyamide PA 12 Smooth), as shown in Figure 6. The picture shows the structure at 10x magnification, together with the so-called "layering" individual layers on the printed part. The disadvantage of this technology is the microscopic porosity, which is visible in the form of small "bright" (white) places.

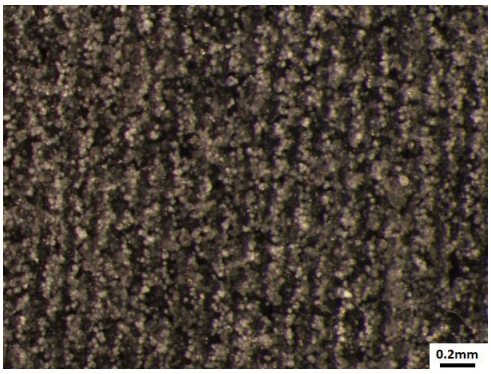

Fig. 6. A printout from the Sinterit LISA printer under a microscope (10x magnification)

The second was a printout from the EOS FORMIGA P100 printer and white Polyamide PA 2200. The structure is shown in Figure 7 at a 10x magnification. Observation of the given sample from a practical point of view showed a light-coloured surface structure with different pigments. At the same time, as with the previously observed sample, it shows "bright" (white) places, which indicates a non-continuous surface with holes.

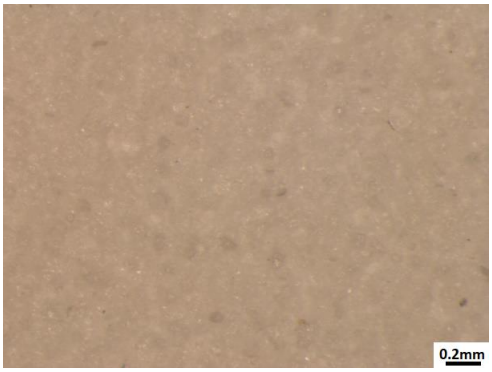

Fig. 7. A printout from the EOS FORMIGA P100 printer under a microscope (10x magnification)

The objects printed on the HP JET Fusion 4200 printer were of high quality and high processing. It is impossible to observe material defects with the naked eye. The rigid and flexible construction of a print made of Polyamide PA12 material provides users with a product with almost isotropic properties throughout the body. Figure 8 shows a detail of the structure of the 3D print-out at 10x magnification.

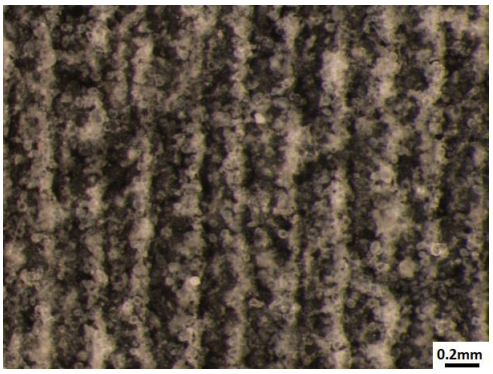

Fig. 8. A printout from the HP printer under a microscope (10x magnification)

3.3. Topography survey of prints

To examine the microstructure, too used the ALICONA Infinite Focus G5 (see Figure 9). This device is a highly accurate and flexible 3D measurement system. It provided the user with an output with an accuracy of up to 10 nm. The advantage of this device is its ability to isolate noise and vibrations, which can negatively affect the measured results. Simultaneously, the device provides a comprehensive view of the topography of the investigated object using various roughness parameters. (ALICONA, 2022)

As designers of the equipment, we were interested in the surface properties of the individual examined prints, in addition to the mechanical properties. Uneven surfaces can negatively affect the degree of disinfection and duration of UV-C radiation. In addition to affecting the strength, the fragmentation of structure surfaces also affects the number of captured bacteria. Inserting a small object can cause the transfer of bacteria to the surface of the device.

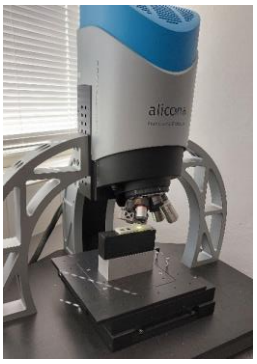

Fig. 9. 3D measuring system ALICONA Infinite Focus G5

Figures 10, 11, and 12 show the prints' primary surfaces at 100x magnification. The extraction of the primary surface was performed using IF-Sensor C100 G1 optics. The white spots in the pictures indicate either material errors or reflected light

rays. This phenomenon was most noticeable in the second sample from the EOS FORMIGA P100 printer.

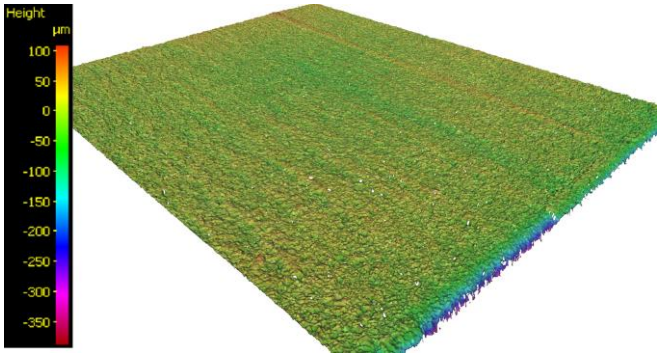

Fig. 10. A view of the primary product surface of the LISA printer

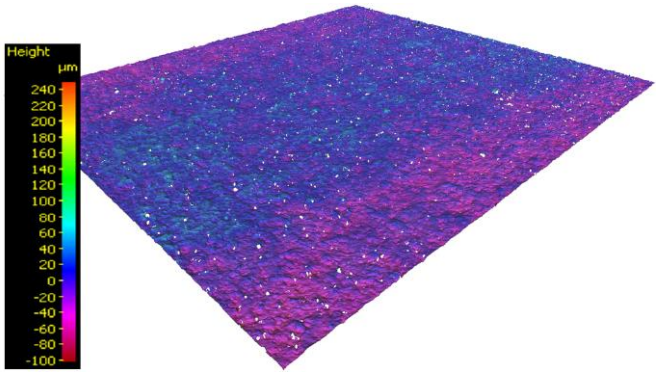

Fig. 11. View of the primary product surface of the EOS Formiga P100 printer

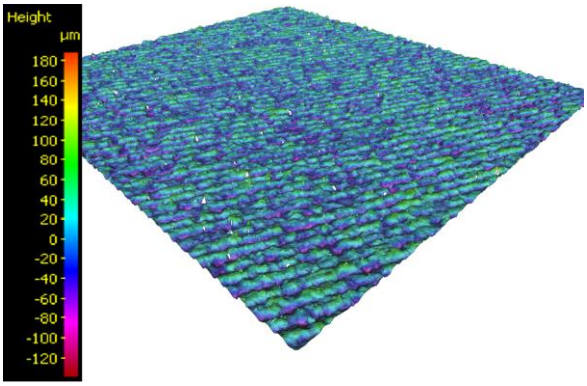

Fig. 12. A view of the primary product surface of the HP Jet Fusion 4200 printer

From the images of the microstructure of the primary surface, it can be observed that the third print (Multi Jet Fusion) has the most readable texture (layering). Figure 12 shows are visible the applied powder layers comprising the given component. An important finding is that the deviations of the primary surface for sample 3 (HP printer) reached the smallest range. Subsequently, the samples were evaluated for 2D roughness. During the investigation, 50 roughness profiles with a length of 1 cm were extracted (see Figure 13, Figure 15, and Figure 17). The graphic course shows the worst parameters in surface functionality (See Figure 14, Figure 16, and Figure 18).

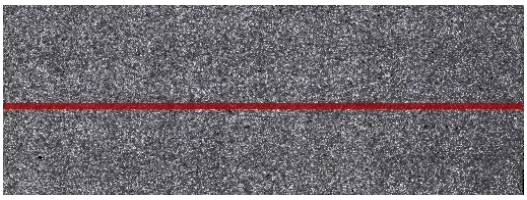

Fig. 13. 2D roughness measurement, selection of the worst surface sample (SINTERIT LISA printer)

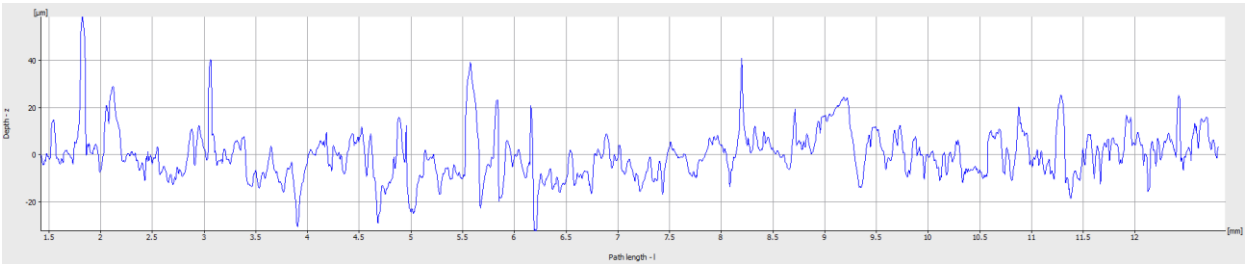

Fig. 14. 2D Roughness on a measured sample from the SINTERIT LISA printer

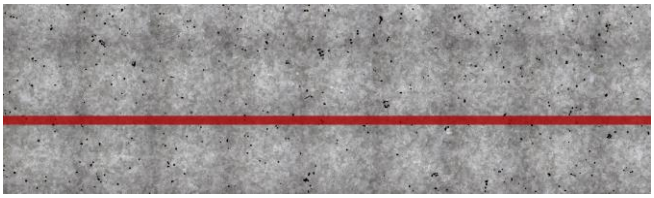

Fig. 15. 2D roughness measurement, selection of the worst surface sample (EOS Formiga P100 printer)

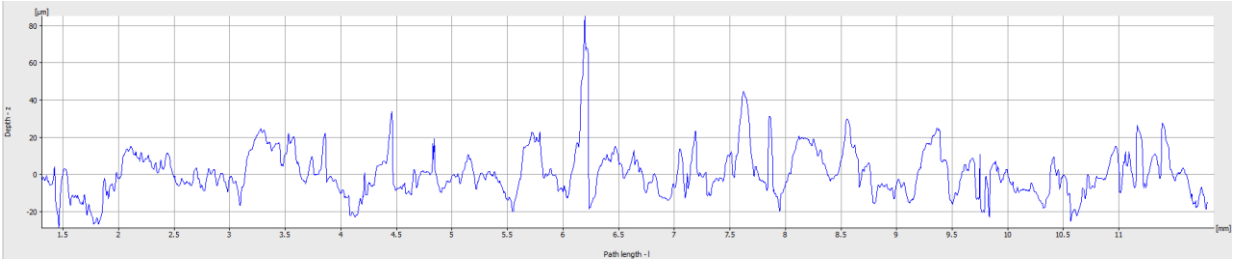

Fig. 16. Roughness on a measured sample from the EOS Formiga P100

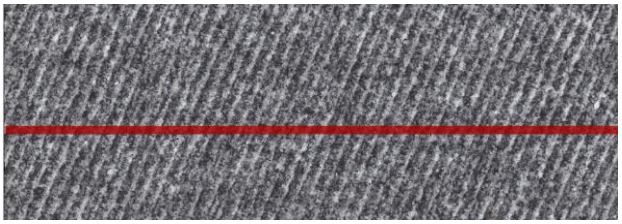

Fig. 17. 2D roughness measurement, selection of the worst surface sample (HP MJF 4200 printer)

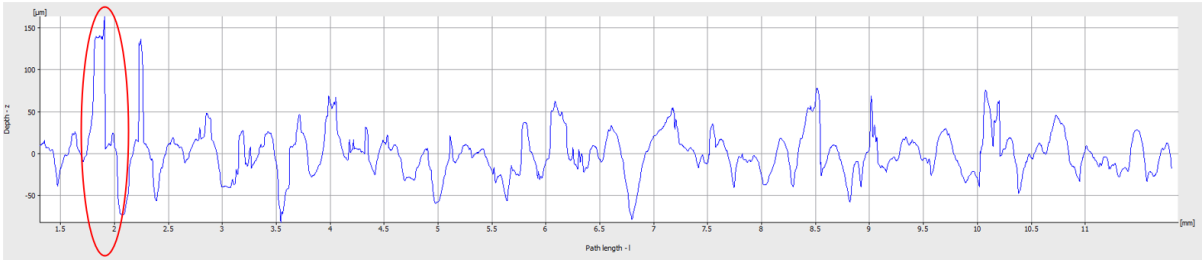

Fig. 18. Roughness on a measured sample from the HP MJF 4200

Based on the presented curves, it can be concluded that the largest amplitude (marked in red) was achieved with the third sample from HP Jet Fusion 4200 (see Figure 18). More details regarding the topography of the test samples or their 3D roughness are shown in Figures 19, 20, and 21. To evaluate the surface topography was set the nesting index to 8µm by applying a Gaussian filter. The colour scale indicates the printed material's increased roughness or defective state.

In Figure 19, it is possible to see how a layer showing signs of increased roughness was carried throughout the entire part. This layer may have resulted from a non-continuous event, sufficient micro-movement, or a slight bang on the table, and this minor defect in the printed part was caused. The more significant section of the 3D printed-out is the same in the picture or a very similar colour. The colour scale indicates a low value of the mean arithmetic deviation of the Ra profile, which is only 7.6567µm (see Table 4).

The continuity and better stability of the surface, although the EOS Formiga P100 printer provided higher roughness (Ra=9.1857) (see Figures 16 and 20). In this print, the surface roughness deviation amplitude did not often reach extreme values in the roughness values. However, the continuity of the surface was disturbed by imperfections in the connections of the individual layers. The local maxima were higher than when printed by the first 3D printer (Synterit LISA).

The differences in the printing are shown on the printed part. The roughness amplitude in Figure 18 reached the value of the mean arithmetic deviation of the profile up to Ra=21.02 (see Table 4). The graph indicates that the part with measured characteristic values resembles an unprocessed semi-finished product. At first glance, the visibility of the layers may appear to be a significant problem in the given issue during prototype creation. However, the high flexibility and the best mechanical properties of products from this printer stand out.

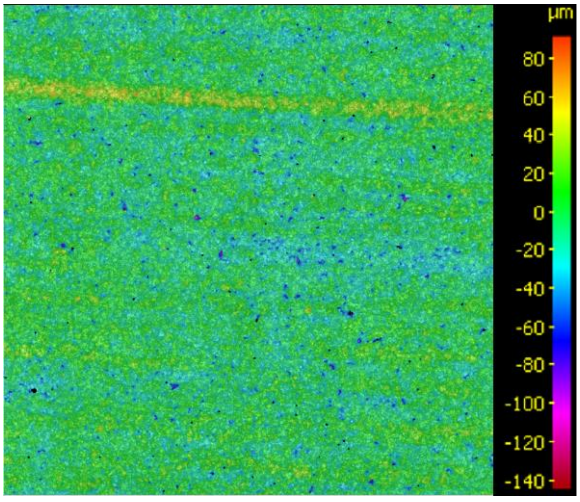

Fig. 19. 3D roughness of the print of the SINTERIT LISA printer

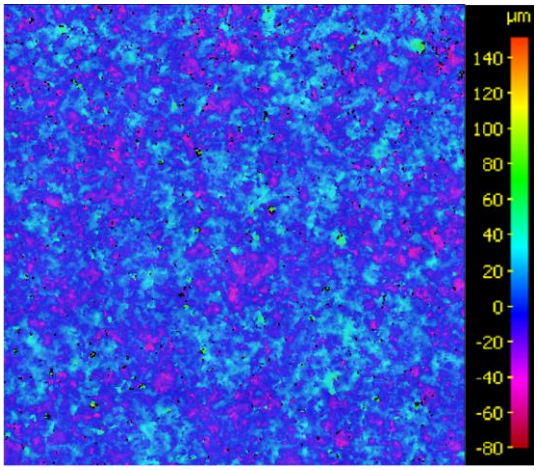

Fig. 20. 3D roughness of the print of the EOS FORMIGA P100

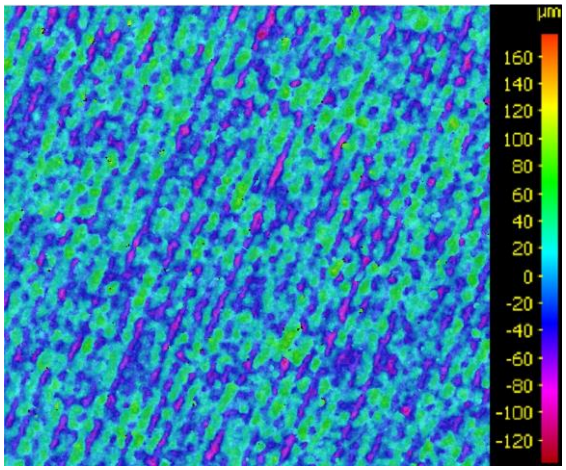

Fig. 21. 3D roughness of the print of the HP MJF 4200

The ratio of the roughness coefficient values Rv/Rz (depth of most considerable profile depression/most significant profile height) is often used to characterize the surface properties. If the value of this coefficient approaches number one, depressions prevail on the surface. This fact may result in a cyclic stress fracture. The presence of pits and holes can indicate locations where bacteria can linger. The ratios of these two values are listed in Table 4. The smallest value of the pk-pk amplitude occurred when the EOS printer was printed. The value of the coefficient of asymmetry of the profile RSK is the authoritative quantity for determining whether protrusions (positive values) or holes/indentations (negative values) predominate. From this point of view, all RSK values are positive; protrusions are predominant. The wave protrusions were most noticeable in the sample from the EOS Formiga P100 printer (see Table IV). The smallest RSK coefficient was by the LISA printer.

Table 4. Roughness values of printed parts

Printer	Ra [µm]	Rv [µm]	Rz [µm]	R_{sk}	R_v/R_z
LISA	7.657	32.195	59.422	0.9596	0.542
EOS	9.186	28.714	66.363	1.4307	0.433
HP	21.204	81.993	157.094	1.2455	0.522

3.4. Evaluating of available prototyping methods

The given technology complies with the specified requirements of the properties of the prototype. The best properties of the print, such as tensile strength, elongation at break, hardness, impact resistance and processing quality, were obtained from the HP (MJF) printer. When comparing printing devices, the printing speed of MJF is high, which is closely related to increased productivity. With SINTERIT LISA, one can not speak of high productivity because of the time required to print objects.

The partner company's HP JET Fusion 4200 3D printer is currently busy with work still. There is a question of economic difficulty in manufacturing the model. From the point of view of the price and availability of the device, production on the HP JET Fusion 4200 printer is more economically demanding than that on the Sinterit LISA and EOS Formiga P100 printers. With this consideration, the question arises of creating a prototype quickly at an acceptable cost.

From the point of view of the length of the printing time, powder production costs, and equipment workload, the EOS Formiga P100 printer is more suitable for the initial design. The topography of the surface, delivery time, and cost favour the EOS Formiga P100 printer. A qualitative examination of the structure surfaces showed insufficient processing of the prints (protrusions prevailed and higher roughness). However, this printer achieved the lowest number regarding the Rv/Rz ratio.

4. FEM analysis and optimization of the key points of the construction

In this case, they can be used the analysis FEM to understand better and visualise how the device can behave under load. This manuscript uses used software ANSYS Workbench for this purpose.

When determining the load of our structure, it is necessary to predict the situation that the device can enter. Considering that the emphasis is also on the mobility of the device is assumed that the construction of the disinfection device can be submitted to various external loads. The device can be submitted to pressure in a bag (luggage), force during unfolding/folding, or accidental falls/impacts/loads. In load cases, it is essential to determine the critical components of the structure. The main task of these crucial components is to transfer the load and hold the system together. Therefore, a more detailed examination of them is necessary.

4.1. Load in the bag

In the case of the disinfection chamber, the elements that make up the folding mechanism are the key components (top cover, bottom cover, pins). Transferring the device can be a point of contention, that is, if the device is in a folded state and forces are acting on it (e.g. in a bag). It is essential to determine how the forces can act and how big the forces can act. The device would be by transporting the upper and lower covers loaded from the sides. Figure 22 shows a visible section of the device with an indication of the action of forces.

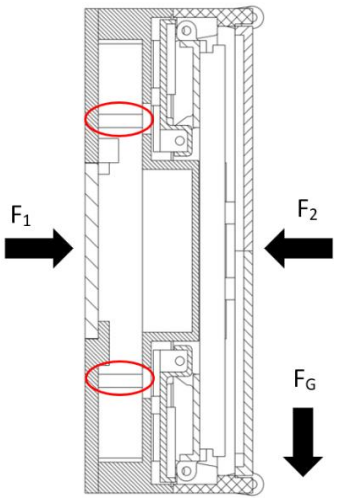

Fig. 22. Disinfection device in section with action forces

With this consideration, there was a need to add reinforcements to the lower part of the device (red ellipses in figure 22). The braces should be positioned where the control and battery module are. The main task of the reinforcements would be the mechanical protection of the mentioned modules. From the point of view of determining the critical parts, the just-mentioned upper and lower covers are crucial. The deflection of components under load could disrupt the functionality of the entire device. Since the emphasis is on mobility, the actual procedure of storing it in the bag should also be described in the device's user manual. Always transport in a folded state and with the shorter edge in a horizontal position, as in figure 22.

For the ordinary load of the bag, it should be noted that the weight of the regular school bag should not exceed 10% of the wearer's weight (Leong, 2021). A study about the current mass of schoolchildren's backpacks (7-9 years old) detected that the weight of one bag is from 4.7kg to 9 kg. (Brzęk et al., 2017; Oosterhoff and Palmet, 2020)

4.2. Material

The material properties are essential for performing FEM analysis. (Caco et al., 2017) Most of the properties are mentioned in Section 3.2.4 in Table 3. The authors wanted to conduct a more in-depth survey of the existing data and articles to summarize when creating the input data for the calculation. The parameters are influenced by the following:

- spacing during movement
- speed of laser movement
- thickness of a deposited layer, and
- the interaction between the spacing during the laser movement and the thickness of a layer. (Wegner and Witt, 2012)

Correlation between properties was sought by Hofland et al. (2017). The authors concluded that the greater the energy acting on the powder, the better the print properties were achieved up to a certain point. The website material-datacenter (2022) shows that several powders are produced (balanced, performance, speed, top quality, and top speed). According to the manufacturer EOS, the density is 930 kg/m3. The value of Young's modulus is between 1650-1700 MPa, and the tensile strength is 48MPa. (material data center, 2022) (EOS, 2022) (Shapeyways, 2021) Authors Faes et al. (2016) tested the properties of PA 12 material when printing on an EOS P395 industrial device. Young's modulus describes the isotropic properties of prints with 1632MPa and Poisson's number of 0,41. Stoia et al. (2019) performed tensile tests on different sintering orientations. The samples failed the most at 12-16% elongation at break and the maximum tensile strength of 33 MPa. Poisson's number raged from 0,39 - 0,42. Due to the absence of data in the ANSYS Workbench database, the authors chose their material with the parameters listed in Table 5.

Table 5. Properties of material in ANSYS Workbench

Material		PA 2200
Properties	Value	Unit
Density	930	kg/cm^3
Melting temperature	176	°C
Isotropic properties		
Tensile modulus (Young modulus)	1650	MPa
Poisson's Ratio	0,41	-
Bulk modulus	3.0556	GPa
Shear modulus	585.11	MPa
Tensile ultimate strength	48	MPa

4.3. FEM Analysis

This chapter described the FEM analysis of a small disinfection chamber. The loads are simulated for the extreme case of bag loads. The device is not in motion and therefore is chosen for static analysis. In the study are linear relation holds between applied forces and displacements. For static analysis, inputs like the model, connections, meshing, and boundary conditions are necessary. The model was uploaded from CREO Parametric 8.0 to ANSYS Workbench as an assembly in step format. The critical holes and rounding were removed from the 3D model to achieve more precise results. These construction elements can act as stress concentrators and cannot affect the results so vehemently.

Parts of the folding mechanism, which are folded in the inner part, have been removed from the assembly model. The influence of these parts on the analysis in terms of the strength of the covers is minimal. But it is relevant to consider how a collision with internal parts can occur and how they can be affected. Since the device is stored in a bag, there is no need for large movements of parts. The connections in the model between plastic parts are BONDED. The contact connections between the plastic parts and the pins are also treated with a BONDED contact. The meshing is essential for the accuracy of the results.

Rounding, chamfering, holes, and other complicated geometry are reasons for using tetrahedron meshing. Because we wanted to know what the fundamental behavior of the device would be under load, it was necessary to leave some rounding on the device parts. The exception in meshing is small steel

pins that are meshed automatically (see Fig. 23). The pins were divided into five parts.

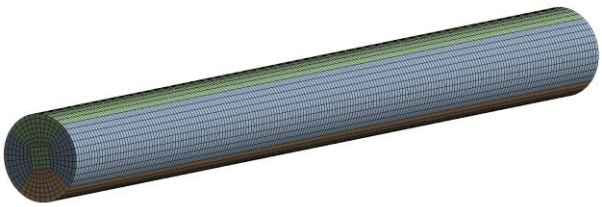

Fig. 23. The meshing of steel pin

The boundary conditions in this simulation are seated for the extreme case of the force actions. In the model was created two small surfaces (on the bottom and the top). These surfaces will simulate areas on which the external and extreme loads act. Dimensions of these areas are 20x20mm. The force acting on the mentioned surfaces was chosen at the value 30N. The magnitude of the force was derived from the weights of the school bags. The A condition of fixed support was established for the lower part of the device (see Fig. 24).

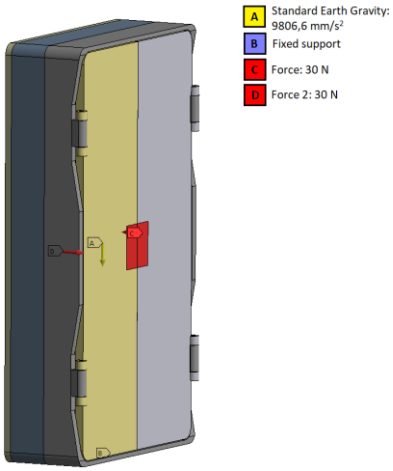

Fig. 24. Boundary conditions

4.3.1. Bottom cover

The bottom cover of the device was reinforced with four supports even before the actual analysis process. This change had a significant impact on strengthening the entire bottom surface of the device. It was necessary to make a section of the part to evaluate the simulation and display the stress and deformation.

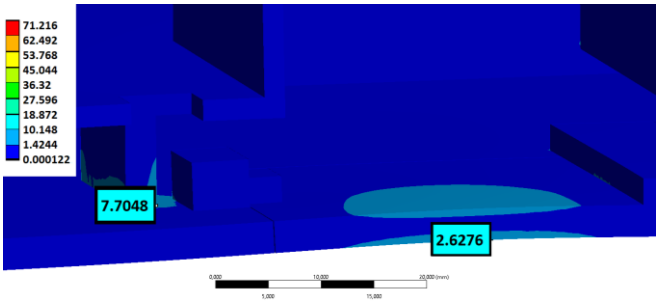

Fig. 25. Equivalent (von Mises) Stress (MPa) - Bottom cover

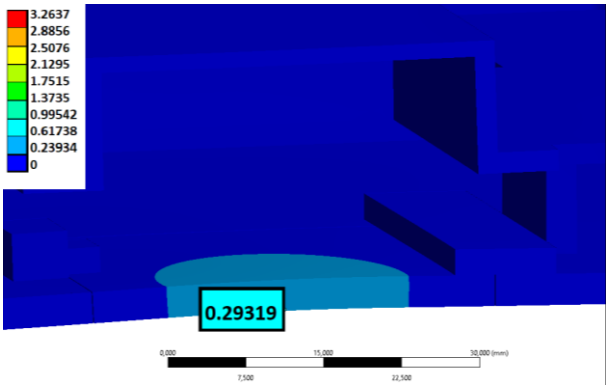

Fig. 26. Deformation - Bottom cover (mm)

Figure 25 shows the Equivalent (von Mises) Stress in the bottom cover of the section. Figure 26 shows the deformation (mm) in the area of the part. The results were significantly affected by the added support. The maximum stresses were based on the supports, in values of up to 4 MPa (see Fig. 26). The maximum deflection in the lower part ranged to 0.3 mm (see Fig. 27).

4.3.2. Top cover

The top cover consists of two openable doors. Rounds and various complex geometric elements have been removed from the model to simplify. Critical in this element is bending the center of the cover, which can affect the parts of the device hidden under the surface (a folding mechanism). Damage to the top of the body can lead to the destruction of the device. From the top cover to other parts in the device is space 4.25mm.

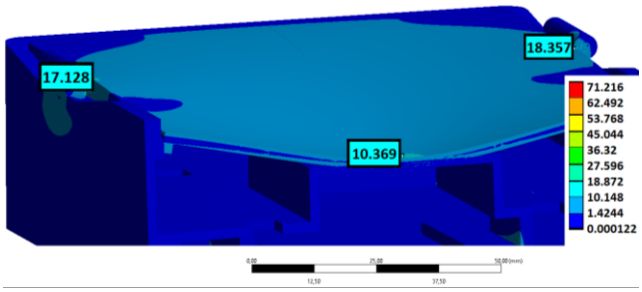

Fig. 27. Equivalent (von Mises) Stress (MPa) – Top cover

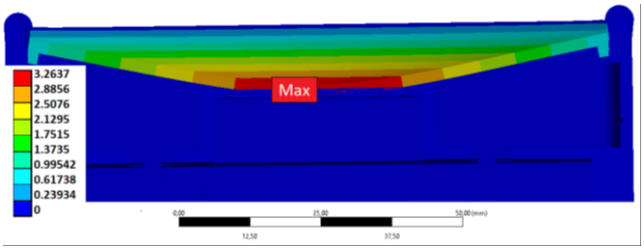

Fig. 28. Deformation (mm) - Top cover

The pins are essential to the device's structure and folding mechanism. It is necessary to know how high the Equivalent (von Mises) Stress on the pins is. The stress reflected an exertion of the pin during the action of critical forces.

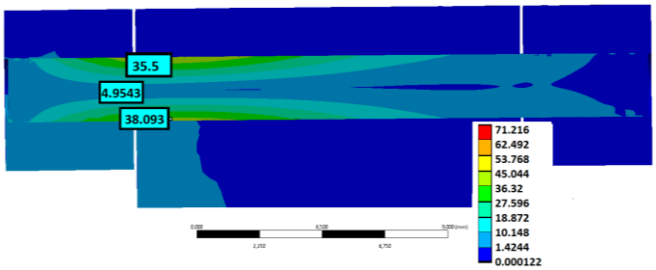

Fig. 29. Equivalent (von Mises) Stress in steel pin (MPa)

The analysis results provide insight into the behavior of the top cover under the action of forces. The maximum equivalent (von Mises) stress on the top of the body is about 10-11 MPa (see Fig. 27). The maximal deformation in this place is about 3.3mm (see Fig. 28). One of the other essential points of the structure and the scalding mechanism are the pins (see Fig. 29) The maximum Equivalent (von Mises) Stress on the pins at the extreme chosen load is around 44 MPa.

4.3.3. Evaluation of analysis

The static analyses performed in this chapter are primarily a source for the preliminary design and verification of the designed dimensions in critical parts of the structure and provide a basis for their possible optimization. For the first time, it is necessary to mention that bonded connections between plastic parts and steel pins influence the analysis results. Secondly, analysis was performed under the action of an extreme load.

For the powder material, it is essential to say that in the several cited works (chapter 4.2), the values measured during tear tests differed from those given by the material manufacturers. These deviations are caused by the manufacturer performing tests with a wholly melted material. The homogeneity and omnidirectional stability are on a high level.

This chapter investigated the folded state of the device. The top (Chapter 4.3.1) and bottom (Chapter 4.3.2) covers under extreme loads exhibited some deflection value. The stress values were not high owing to the considerable elasticity of the printed material. Before the analysis, was made changes in construction. Were designed four struts to support the bottom cover. This step eliminated deflections and possible collisions in the structure when extreme loads were applied. The collision of parts can be seen in Figure 27 and Figure. 29 (Chapter 4.3.2). According to the results, iron pins should transmit force and withstand extreme load cases. At the actual deflection value, however, contact should not occur at all (software). The deflection of the top cover cannot affect the device's functionality.

This chapter pointed out the importance of analysis in the preliminary design of the structure. The presented static analysis results should be taken as an aid in dimensioning and designing. The accuracy of the results is significantly influenced by the connections, mesh, and material properties.

5. Results – Mechanical design of the device

Based on previous research, we developed a prototype mobile disinfection chamber for small communication devices and objects. The prototype was characterized by mobility and stack ability (see Figures 30 and 31). The prototype was produced using the SLS method with an EOS Formiga P100 3D printer.

The device weight without mounting elements, only printed parts, is 252.2g. Together with the rotating steel pins, it should be approximately 260g. This weight does not include the battery module or the entire electrical part/module (lighting and control elements).

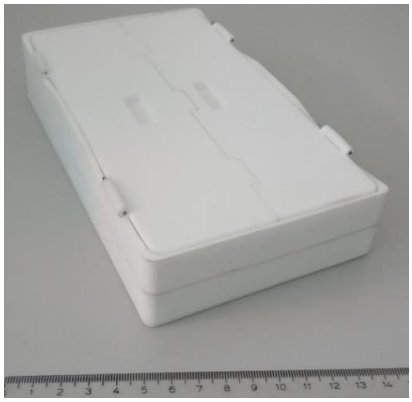

Fig. 30. The resulting mechanical part of the device in a closed and folded state

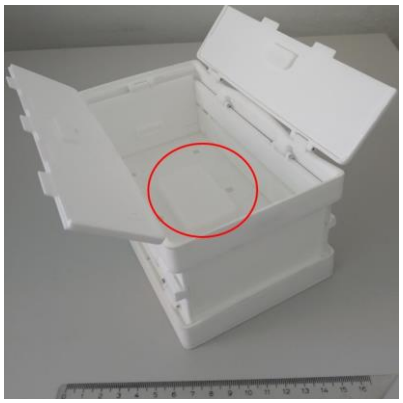

Fig. 31. The resulting mechanical model of the device in a disassembled and open state

Steel pins and screws were used as the connecting elements in the prototype versions. In further developments, the authors do not limit themselves to other methods of securing mechanisms within the structure. In this case, it is also necessary to mention other materials (composites, possibly aluminium, etc.) that would reduce the device's weight.

During the design of the new concept, it was necessary to pay attention to the missing electrical part and create conditions for applying the electrical module of the given device. In Figure 40 (highlighted in red), it is possible to see a niche in the structure, which, from a functional point of view, forms a case for fitting a battery module, that would power the circuit with LED lights. At the same time, the protrusion forms a base for the inserted objects, making it possible to maintain the distance between the inserted object and the source of UV-C radiation. With this offset, a larger object area was exposed to UV-C radiation.

6. Discussion

Unfolding, inserting, and selecting objects from the device can influence the user's using a new appliance. The material properties, surface design, roughness, strength, and durability are relevant properties of the designed device. The appearance and design, together with the aspect of roughness, will influence the user so that the device can be more user-friendly.

Low weight is one of the most relevant features that influence the frequency of use. It is, therefore, vital to address this issue. Choosing the correct ratio of strength to total weight is even more essential. Users are in demand, and devices must be durable and lightweight while performing their functions. The design (appearance of the device) dramatically influences the use of the device. The friendliness of the design, combined with round lines and integral curves that form the edge of the product, is another aspect of the device's success.

The sources of UV-C radiation and their effects on the inserted object (disinfection) cannot be neglected. For the device to work correctly and disinfect surfaces, it must be said that the inserted object should be exposed to UV-C radiation from all sides as much as possible. Radiation sources were also added to the construction side or first folding cover. The connection between the UV-C LED bulb and the power supply/control appears critical. There has been an effort to create a guide channel to maintain functionality.

Several researchers have investigated the polyamide materials in this manuscript within the Faculty of Mechanical Engineering Research Centre. A team of researchers also dealt with developing a device for disinfecting factories' production areas by using a UV-C module mounted on an automated guided vehicle (AGV) cover.

7. Conclusion

The presented article provides the reader with an insight into the process of constructing a new device that is beneficial to society. The proposed device's main task is fighting against dangerous pathogens on small objects of daily use. It is assumed that the use of this device would lead to increased protection of the population associated with a high degree of portability of the device.

An introduction to the article was formulated by theoretical knowledge and surveying the current state of the market. The essential part of this manuscript is the design process of solution variants. (Chapter 2) The final solution of the product can significantly affect the implementation methods, so it's important to pay sufficient attention to this process. The evaluation process determined the most suitable variant and proceeded to select the right, above all, available production method (Chapter 3). The most suitable variant was chosen using the ALICONA Infinite Focus G5 device.

At the end (chapter 4) was made a FEM analysis with some device modifications. The analysis had a recommendation character. Described essential parts of the device, such as the bottom cover, top cover, and steel pin, lasted to withstand extreme forces. At the end of the article (chapter 5), there is a described real printed model of the device.

The research should continue with other optimization processes and actual load test processes. The tests should increase the collapsibility, tightness (transmission of light), and strength - stiffness of the structure. One of the following steps should also be manufacturing a prototype using the MJF method, which is currently unavailable in our laboratory.

The limitation of the presented research is the just-mentioned availability of production methods. If there is an interest in the application of the device and the production of a small series, then the MJF production method is very suitable. It is relevant to mention that the physical properties of prints can be very diverse in different parts. It is affected by various parameters such as models, print speed, bed heating, etc. Of course, if we want to have the device functional, the availability of parts for the electrical and battery modules becomes essential.

Further development should lead to research on disinfection capabilities and the developing device's electrical module. The research and development should be focused module's design with the PCB, controlled charging, safety features, on/off buttons, battery status, and others. The module's implementation depends on the dimensional options and the weights of new parts. The main goal is to make the device a complex product. The primary function is combining simplicity and high efficiency in one device.

Acknowledgements

This article was funded by the University of Žilina project 313011ASY4— "Strategic implementation of additive technologies to strengthen the intervention capacities of emergencies caused by the COVID-19 pandemic."

Reference

ALICONA, 2022. Dimensional accuracy & surface finish measurement. available at: https://www.alicona.com/products/infinitefocus/ (Accessed 10 April 2022).

Baloch, S., Baloch, M. A., Zheng, T., and Pei, X., 2020. The Coronavirus Disease 2019 (COVID-19) Pandemic. The Tohoku Journal of Experimental Medicine, 250 (4), 271–278, DOI: 10.1620/tjem.250.271

Bergman, R.S. 2021. Germicidal UV Sources and Systems. Photochemistry and Photobiology, 97(3), 466-470, DOI: 10.1111/php.13387

Brzęk, A., Dworrak, T., Strauss, M., Sanchis-Gomar, F., Sabbah, I., Dworrak, B. and Leischik, R., 2017. The weight of pupils' schoolbags in early school age and its influence on body posture. BMC Musculoskelet Disord, 18 (1), 117, DOI: 10.1186/s12891-017-1462-z

Bukłaha, A., Wieczorek, A., Kruszewska, E., Majewski, P., Iwaniuk, D., Sacha, P., Tryniszewska, E. and Wieczorek, P., 2022. Air Disinfection—From Medical Areas to Vehicle. Front. Public Health, 10, 820816, DOI: 10.3389/fpubh.2022.820816

Caco, M., Tribula, R., Scerba, P.; Kohar, R., 2017. Application of simulation software to optimize construction nodes of ultrasonic welding machines. Proceedings of 58th international conference of machine design departments (ICMD 2017), Prague, Czech University of Life Sciences Prague, 56-59.

CDC, 2015. Hierarchy of Controls. available at: https://www.cdc.gov/niosh/topics/hierarchy/default.html (accessed 15 April 2022)

CDC, 2021. Cleaning and Disinfecting Your Facility. available at: https://www.cdc.gov/coronavirus/2019-ncov/community/disinfecting-building-facility.html (accessed 03 May 2022)

Chen, X., Liao, B., Cheng, L., Peng, X., Xu, X., Li, Y., Hu, T., Li, J., Zhou, X., and Ren, B., 2020. The microbial coinfection in COVID-19. Applied Microbiology and Biotechnology, 104(18), 7777–7785, DOI: 10.1007/s00253-020-10814-6

Engineering product design, 2022. Rapid prototyping. available at: https://engineeringproductdesign.com/knowledge-base/rapid-prototyping-techniques/ (accessed 18 March 2022)
EOS, 2007. Technical Description FORMIGA P 100. available at: https://webbuilder5.asiannet.com/ftp/2684/TD_P100_en.pdf (accessed 20 April 2022)
EOS, 2022. Polyamide 12 for 3D Printing. available at: https://www.eos.info/en/additive-manufacturing/3d-printing-plastic/sls-polymer-materials/polyamide-pa-12-alumide (accessed 08 March 2022)
ESA, 2013. 3D printing for space: the additive revolution. available at: https://www.esa.int/Science_Exploration/Human_and_Robotic_Exploration/Research/3D_printing_for_space_the_additive_revolution (accessed 15 April 2022)
European Council, 2022. COVID-19: the EU's response in the field of public health. available at: https://www.consilium.europa.eu/en/policies/coronavirus/covid-19-public-health/ (accessed 05 April 2022)
Faes, M., Wang, Y., Lava, P. and Moens, D., 2016. Variability, heterogeneity, and anisotropy in the quasi-static response of laser sintered PA12 components. Strain An International Journal for Experimental Mechanics, 53(2), DOI: 10.1111/str.12219.
FAO, IFAD, UNICEF, WFP and WHO, 2020. The State of Food Security and Nutrition in the World 2020. Rome, Italy.
Furka, S., Furka, D., Dadi, N. Ch. T. Ch. T., Palacka, P., Hromníková, D., Santana, J. D. S., Pineda, J. D., Casas, S. D., and Bujdák, J., 2021. Novel antimicrobial materials designed for the 3D printing of medical devices used during the COVID-19 crisis. Rapid Prototyping Journal, 27(5), 890-904, DOI: 10.1108/RPJ-09-2020-0219
Gan, X., Fei, G., Wang, J., Wang, Z., Lavorgna, M., Xia, H., 2020. Powder quality and electrical conductivity of selective laser sintered polymer composite components. Woodhead Publishing Series in Composites Science and Engineering Part 2, Elsevier, Woodhead Publishing, 149-185.
Gibson, I., Rosen, D., Stucker, B., 2014. Additive Manufacturing Technologies. New York: Springer.
Groth, L., 2020. 9 Vitamin D Benefits You Should Know—and How to Get More in Your Diet. Health, 25 June, available at: https://www.health.com/nutrition/vitamins-supplements/vitamin-d-benefits (accessed 10 May 2022)
Hofland, E.C., Baran, I., Wismeijer, D.A., 2017. Correlation of Process Parameters with Mechanical Properties of Laser Sintered PA12 Parts. Advances in Materials Science and Engineering, 2017(4953173), 1-11, DOI: 10.1155/2017/4953173
HP, 2022. HP Jet Fusion 4200 Industrial 3D Printing Solution. available at: https://www.hp.com/us-en/printers/3d-printers/products/multi-jet-fusion-4200.html (accessed 20 may 2022)
Hsu, T.C., Teng, Y.T., Yeh, Y.W., Fan, X., Chu, K.H., Lin, S.H., Yeh, K.K., Lee, P.T., Lin, Y., Chen, Z., Wu, T., Kuo, H.C., 2021. Perspectives on UVC LED: Its Progress and Application. Photonics, 8(6), 196, DOI: 10.3390/photonics8060196
JAG Jakob SA, 2020. Selective UV-C disinfection on autonomous mobile robot (AGV - AMR). available at: https://www.siams.ch/news-en/selective-uv-c-disinfection-on-autonomous-mobile-robot--agv---amr-/4023 (accessed 23 May 2022)
Khorasani, M., Ghasemi, A., Rolfe, B. and Gibson, I., 2022. Additive manufacturing a powerful tool for the aerospace industry. Rapid Prototyping Journal, 28(1), 87-100, DOI: 10.1108/RPJ-01-2021-0009.
Kitagawa, H., Nomura, T., Nazmul,T., Omori, K., Shigemoto, N., Sakaguchi, T. and Ohge, H., 2021. Effectiveness of 222-nm ultraviolet light on disinfecting SARS-CoV-2 surface contamination, American Journal of Infection Control, 49(3), 299-301, DOI: 10.1016/j.ajic.2020.08.022
Kohár, R., Stopka, M., Weis, P., Spišák, P., Šteininger, J., 2020. Modular 3D Printer Concept, Current Methods of Construction Design. Lecture Notes in Mechanical Engineering, ICMD 2018, Cham, Springer, 483-488.
Leong, A., 2021. School Bags Shouldn't Weigh More Than 10% Of The Child's Weight, Says Study. available at: https://www.therakyatpost.com/news/2021/12/01/school-bags-shouldnt-weigh-more-than-10-of-the-childs-weight-says-study/ (accessed 02 June 2022)
Lewis, D., 2020. Is the coronavirus airborne? Experts can't agree. Nature, 580, 175
Luyster, F.S., Strollo, P.J., Zee, P.C. and Walsh, J.K., 2012. Sleep: A Health Imperative. Sleep, 35(6), 727-734, DOI: 10.5665/sleep.1846
Ma, B., Gundy, P.M., Gerba, Ch.P., Sobsey, M.D. and Linden, K.G., 2021. UV Inactivation of SARS-CoV-2 across the UVC Spectrum: KrCl* Excimer. Mercury-Vapor, and Light-Emitting-Diode (LED) Sources, Applied and Environmetal Microbiology, 87(22), DOI: 10.1128/AEM.01532-21
Material datacenter, 2022. PA 2200 Balance 1.0. available at: https://www.materialdatacenter.com/mb/material/pdf/30962/30962/PA2200Balance1.0 (accessed 14 June 2022)
Materialize, 2022. Powder based 3D printing, without the lasers. available at: https://www.materialise.com/en/manufacturing/3d-printing-technology/multi-jet-fusion (accessed 03 June 2022)
Mehrpouya, M., Tuma, D., Vaneker, T., Afrasiabi, M., Bambach, M. Gibson I., 2022. Multimaterial powder bed fusion techniques. Rapid Prototyping Journal, 28(11), 1-19, DOI: 10.1108/RPJ-01-2022-0014
Mohol, S.S., Sharma, V., 2021. Functional applications of 4D printing: a review. Rapid Prototyping Journal, 27(8), 1501-1522, DOI: 10.1108/RPJ-10-2020-0240
Morawska, L., Cao, J., 2020. Airborne transmission of SARS-CoV-2: The world should face the reality. Environment International, 139, 105730, DOI: 10.1016/j.envint.2020.105730
National Environment Agency, 2021. Guidelines for In-House Cleaning and Disinfection of Areas Exposed to COVID-19 Cases in Non-Healthcare Premises. available at: https://www.nea.gov.sg/our-services/public-cleanliness/environmental-cleaning-guidelines/guidelines/guidelines-for-in-house-cleaning-and-disinfection-of-areas-exposed-to-covid-19-cases-in-non-healthcare-premises (accessed 03 April 2022)
Nourazzaran, M., Yousefi, R., Moosavi-Movahedi, A., 2022. Effects of Vitamin D in Fighting COVID-19 Disease. Iranian J Nutr Sci Food Technol, 16 (4), 121-130, URL: https://nsft.sbmu.ac.ir/article-1-3294-en.html&sw=Effects+of+Vitamin+D+in+Fighting
Obi, M.U., Pradel, P., Sinclair, M., Bibb, R., 2022. A bibliometric analysis of research in design for additive manufacturing. Rapid Prototyping Journal, 28(5), 967-987, DOI: 10.1108/RPJ-11-2020-0291
Oosterhoff, B. and Palmer, C.A., 2020. Psychological Correlates of News Monitoring, Social Distancing. Disinfecting, and Hoarding Behaviors among US Adolescents during the COVID-19 Pandemic, PsyArXiv Preprints, 174(12), 1184-1190, DOI: 10.31234/osf.io/rpcy4
Ouajjani, K., 2018. The History of 3D Printing. available at: https://www.engineeringclicks.com/history-of-3d-printing-2/ (accessed 10 April 2022)
Philips Box, 2022. UV-C disinfection box 10L TG GM. available at: https://www.lighting.philips.com.sg/consumer/p/disinfection-disinfection-box/8719514302259 (accessed 15 April 2022)
Philips Minibox, 2022. UV-C disinfection mini box G GM. available at: https://www.lighting.philips.com.ph/consumer/p/disinfection-disinfection-box/8719514344846 (accessed 15 April 2022)
Philips UV-C, 2022. Protect your home against viruses and bacteria with UV-C lighting. available at: https://www.lighting.philips.co.uk/consumer/uv-c-lighting (accessed 16 April 2022)
Ruschel, J., Glaab, J., Susilo, N., Hagedorn, S., Walde, S., Ziffer, E., Cho, H. K., Ploch, N. L., Wernicke, T., Weyers, M., Einfeldt, S. and Kneissl, M., 2020. Reliability of UVC LEDs fabricated on AlN/sapphire templates with different threading dislocation densities. Applied Physics Letters, 117(24), 241104, DOI: 10.1063/5.0027769
Sculpteo, 2021. 3D Printing with Multi Jet Fusion technology. available at: https://www.sculpteo.com/en/materials/jet-fusion-material/ (accessed 01 June 2022)
Shapeyways, 2021. Access EOS Selective Laser Sintering with Shapeways. available at: https://www.shapeways.com/partnership/eos (accessed 08 June 2022)
Sharma, P., Chen, P., Han, S., Chung, P., Chen, J., Tseng, J. and Han, Ch., 2021. Design Considerations for a Surface Disinfection Device Using Ultraviolet-C Light-Emitting Diodes. Journal of Research of the National Institute of Standards and Technology, 126, 126045, DOI: 10.6028/jres.126.045
SHINING 3, 2022. EinScan-SP SPECS Destkop 3D Scanner. available at: https://www.einscan.com/desktop-3d-scanners/einscan-sp/einscan-sp-specs/ (accessed 16 May 2022)
Sinterit, 2022. Sinterit Lisa SLS 3D printer - the most compact SLS 3D printer. available at: https://sinterit.com/3dprinters/lisa/ (accessed 20 May 2022)
Stoia, D.I., Linul, E., Marsavina, L., 2019. Influence of Manufacturing Parameters on Mechanical Properties of Porous Materials by Selective Laser Sintering. Materials (Basel), 12(6), 871, DOI: 10.3390/ma12060871
Student Lesson, 2022. Understanding non-traditional machining process. available at: https://studentlesson.com/definition-application-diagram-

types-methods-advantages-and-disadvantages-of-non-traditional-machining-processes/ (accessed 09 June 2022)
Tropp, M., Tomasikova, M., Bastovansky, R., Krzywonos, L., Brumercik, F., 2017. Concept of deep drawing mechatronic system working in extreme conditions. 12th International Scientific Conference of Young Scientists on Sustainable, Modern and Safe Transport, High Tatras, Elsevier, 893-898.
Wegner, A., Witt, G., 2012. Correlation of Process Parameters and Part Properties in Laser Sintering using Response Surface Modeling. in Schmidt, M., Vollertsen, F. and Geiger, M. (Ed.s), LANE 2012: Laser Assister Net shape Engineering 7, Furth, Germany, 480-490.
Wiberg, A., Persson, J., Ölvander, J., 2021. An optimisation framework for designs for additive manufacturing combining design, manufacturing and post-processing. Rapid Prototyping Journal, 27(11), 90-105, DOI: 10.1108/RPJ-02-2021-0041
Wu, J., Song, S., Cao, H. C., Li, L. J., 2020. Liver diseases in COVID-19: Etiology. treatment and prognosis, World Journal of Gastroenterology, 26(19), 2286–2293, DOI: 10.3748/wjg.v26.i19.2286

设计和优化小型通信设备和小型物体的移动消毒室的结构

關鍵詞
病原体
紫外线-C辐射
消毒
增材制造
快速原型制作

摘要
本稿件旨在让读者熟悉一种用于小型通信设备和小型物体的移动消毒室的构造的发展。新装置的概念设计和材料在新装置的设计过程中起着至关重要的作用。该手稿主要根据以往的经验和不同的观点提出了概念。概念设计是在三维建模程序CREO Parametric 8.0中创建的。一个多标准的团队评估确定了最合适的概念版本。对于设备的尺寸和形状调整，使用了EinScan SP设备（3D扫描方法）。文章的目的也是为了建立一个合适的方法，在快速成型的范围内，利用现有的生产方法和材料的摩擦学研究来生产一个原型。使用ALICONA Infinite Focus G5设备，通过实验调查了零件表面的特征参数。手稿的结尾集中在机械结构上，并在ANSYS Workbench程序中对其进行有限元分析。概念消毒装置的设计也是为了在极端情况下使用。在这个问题中，利用有限元分析对形状、壁厚、加固设计和其他必要的修改进行了优化。从结果来看，生产更多数量的零件的最合适的材料可能不是创建原型装置的最合适的材料。三维扫描、快速成型和有限元分析等工具可以 "显著 "帮助减少装置测试前的错误